THE JOURNAL OF PHYSICAL CHEMISTRY A

Article

pubs.acs.org/JPCA

Shock Wave Study of the Thermal Dissociations of C_3F_6 and c-C_3F_6. I. Dissociation of Hexafluoropropene

C. J. Cobos,[†] L. Sölter,[‡] E. Tellbach,[‡] and J. Troe*[,‡,§]

[†]INIFTA, Facultad de Ciencias Exactas, Universidad Nacional de La Plata, La Plata, Argentina

[‡]Institut für Physikalische Chemie, Universität Göttingen, Tammannstrasse 6, D-37077 Göttingen, Germany

[§]Max-Planck-Institut für Biophysikalische Chemie, Am Fassberg 11, D-37077 Göttingen, Germany

ABSTRACT: The thermal dissociation of C_3F_6 was studied between 1330 and 2210 K in shock waves monitoring the UV absorption of CF_2. CF_2 yields of about 2.6 per parent C_3F_6 were obtained at reactant concentrations of 500−1000 ppm in the bath gas Ar. These yields dropped to about 1.8 when reactant concentrations were lowered to 60 ppm. The increase of the CF_2 yield with increasing concentration was attributed to bimolecular reactions between primary and secondary dissociation products. Quantum-chemical and kinetic modeling calculations helped to estimate the contributions from the various primary dissociation steps. It was shown that the measurements correspond to unimolecular reactions in their falloff range. Falloff representations of the rate constants are given, leading to an overall high pressure rate constant $k_\infty = 2.0 \times 10^{17}(-104 \text{ kcal mol}^{-1}/RT)\ \text{s}^{-1}$ and a relative rate of about 2/3:1/3 for the reactions $C_3F_6 \rightarrow CF_3CF + CF_2$ versus $C_3F_6 \rightarrow C_2F_3 + CF_3$.

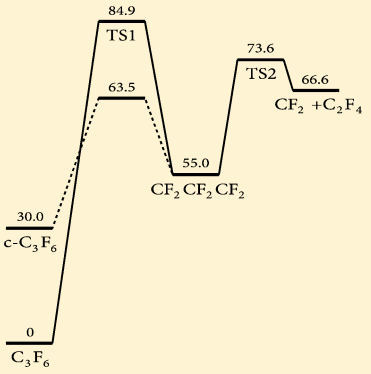

1. INTRODUCTION

The dissociation of hexafluoropropene (C_3F_6) proceeds on several pathways which have been accessed by a variety of activation schemes. In the UV photolysis of C_3F_6 at 193 nm using photofragment translational spectroscopy,[1] CF_2, F, and CF_3 were identified as primary products. Branching fractions of 0.42:0.41:0.17, respectively, were determined. Complementary to this work were studies of the IR multiphoton dissociation[2,3] in which CF_3CF (or C_2F_4), CF_2, and CF_3 were identified as primary dissociation products with branching fractions of CF_2:CF_3 of 0.8:0.2. Assuming that the dissociation in both cases takes place from vibrationally highly excited electronic ground state molecules, these products were attributed to the channels

$$C_3F_6 \rightarrow CF_3CF + CF_2 \qquad \Delta H_0^\circ \approx 104 \text{ kcal mol}^{-1} \qquad (1)$$

$$C_3F_6 \rightarrow CF_3CFCF + F \qquad \Delta H_0^\circ \approx 124 \text{ kcal mol}^{-1} \qquad (2)$$

$$C_3F_6 \rightarrow CF_3 + C_2F_3 \qquad \Delta H_0^\circ = 109.8 \text{ kcal mol}^{-1} \qquad (3)$$

while the thermochemically most favorable channel would be

$$C_3F_6 \rightarrow C_2F_4 + CF_2 \qquad \Delta H_0^\circ = 67.9 \text{ kcal mol}^{-1} \qquad (4)$$

(reaction enthalpies are obtained either from refs 1 and 4 or from G4 calculations of the present work, see Appendix). The latter pathway, however, was estimated[5] to involve an energy barrier of the order of 80−90 kcal mol^{-1}. The isomerization

$$CF_3CF \rightarrow C_2F_4 \qquad \Delta H_0^\circ \approx 16.6 \text{ kcal mol}^{-1} \qquad (5)$$

which follows reaction 1, has been characterized[6] by an energy barrier of 37.5 kcal mol^{-1}.

UV photolysis and IR multiphoton dissociation do not involve the same energy distributions. In addition, the latter differ also from thermal distributions. It would, therefore, be desirable to compare the results with branching fractions and absolute rate constants from thermal dissociation experiments. Although a series of studies gave information on the overall pyrolysis of C_3F_6 (e.g., refs 7−13, see in particular the detailed analysis by ref 5), the results do not appear unambiguous, partly because information on rates and pathways was extracted from complex mechanisms with final product analysis only. A more direct access to the primary thermal dissociation steps appears possible in pyrolysis experiments in shock waves employing the very sensitive detection of CF_2 by UV absorption spectroscopy. This is the method of the present work. CF_2 on one hand is "close to the primary dissociation", and on the other hand secondary reactions can be identified by varying the concentration of the primary reactant. We have already used the detection of CF_2 in a series of earlier dissociation studies of fluoro- and hydrofluorocarbon species like CF_3 and CF_2,[14] CF_3H,[15] C_2F_4,[16] C_2F_5H,[17] C_2F_6,[18] and C_3F_7H.[17] After careful recalibration of the absorption coefficient of CF_2 at 248 nm over a wide temperature range in ref 16, absolute CF_2 yields now can be measured accurately in addition to kinetic data. The present work takes advantage of these previous studies.

The variety of competing dissociation pathways complicates the analysis of the pyrolysis mechanism. Depending on the temperature and the pressure, the loose activated complex-bond fissions (1)−(3) may (or may not) dominate over the rigid

Received: February 13, 2014
Revised: June 6, 2014

   dx.doi.org/10.1021/jp501569a | J. Phys. Chem. A XXXX, XXX, XXX−XXX

activated complex process (4) with its lower threshold energy. In addition, the dissociation is a multichannel process, whose channels influence each other. It, therefore, appears obligatory to accompany the experiments by quantum-chemical calculations of energy profiles and by modeling in terms of unimolecular rate theory. Such combined studies have been made also in our earlier work.[16−18] Another aspect makes this work attractive. The dissociation of hexafluoropropene is related to the dissociation of hexafluorocyclopropane (c-C_3F_6). The two reactions may (or may not) involve the same intermediate.[19−23] Therefore, in a companion article[24] (part II of this series) we report our results on the pyrolysis of c-C_3F_6. There have been conflicting propositions about the energy profiles of the two dissociation processes[5,19,20,25] such that we did new quantum-chemical calculations. As the two systems have markedly different kinetic properties, it appeared appropriate to split the material into two separate articles. However, as the two reactions may (or may not) involve the same $CF_2CF_2CF_2$ intermediate (a 1−3 biradical of the form of a "bond-stretched invertomer"[23]), their intrinsic dynamics may be linked under conditions where process (4) dominates. We aim for an identification of these conditions.

2. EXPERIMENTAL TECHNIQUE AND RESULTS

The dissociation of C_3F_6 was investigated in incident and reflected shock waves. Our shock tube and the applied technique were described before, see, e.g., refs 14−18. The progress of reaction exclusively was followed by light absorption of the forming CF_2 at 248 nm. Absolute values of the absorption coefficient ε at this wavelength were taken from ref 16. The large values of ε (of the order of 3×10^6 cm^2 mol^{-1}, base e) allowed us to work with high dilution of the reactant in the carrier gas Ar. We varied the reactant concentration in Ar between about 60 and 1000 ppm. Ar of 99.9999% purity (from Air Liquide) and C_3F_6 (>99% from acr) were employed. The pyrolysis was studied between about 1330 and 2210 K. Ar concentrations were varied between about 2×10^{-6} and 10^{-4} mol cm^{-3}. The reactions were monitored between about 10 μs and 1 ms.

Kinetic data were obtained from two types of observations. At higher temperatures and shorter reaction times, CF_2 formation was followed until a final level was attained which remained constant up to 1 ms, i.e., the limit of our observation time. At lower temperatures, CF_2 formation was not complete during this observation time. In the former case, CF_2 absorption−time profiles followed a first-order rate law given by

$$[CF_2] = [CF_2]_{t=\infty}\{1 - \exp(-kt)\} \quad (6)$$

Figure 1 shows an example of CF_2 formation behind a reflected shock wave at T = 1727 K, [Ar] = 6.7×10^{-5} mol cm^{-3}, and 530 ppm of C_3F_6. With concentrations of 300−1000 ppm, the final CF_2 yields were found to be

$$[CF_2]_{t=\infty}/[C_3F_6]_{t=0} = 2.6(\pm 0.4) \quad (7)$$

At lower reactant concentrations (of the order of 60 ppm), the CF_2 yields decreased to values of $[CF_2]_{t=\infty}/[C_3F_6]_{t=0}$ = 1.8 (±0.3), see below. A yield of 3 CF_2 per C_3F_6 decomposed could be explained by reaction 4 followed by the fast decomposition of C_2F_4. However, because there is evidence for contributions from reactions 1−3 (see refs1−3, 10, and11), the reduction of the CF_2 yield may also be due to a more complex mechanism involving these reactions, see below. By working behind incident shock waves, we could investigate lower bath gas concentrations. Figure 2 gives an example with T = 1876 K, [Ar] = 1.4×10^{-5} mol cm^{-3}, and

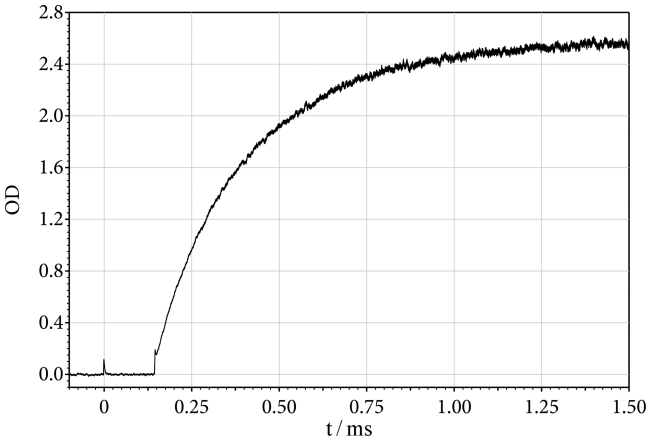

Figure 1. Absorption−time profile (at 248 nm) of the formation of CF_2 in the dissociation of C_3F_6 behind a reflected shock wave (T = 1727 K, [Ar] = 6.7×10^{-5} mol cm^{-3}, $[C_3F_6]_0/[Ar]$ = 530 ppm).

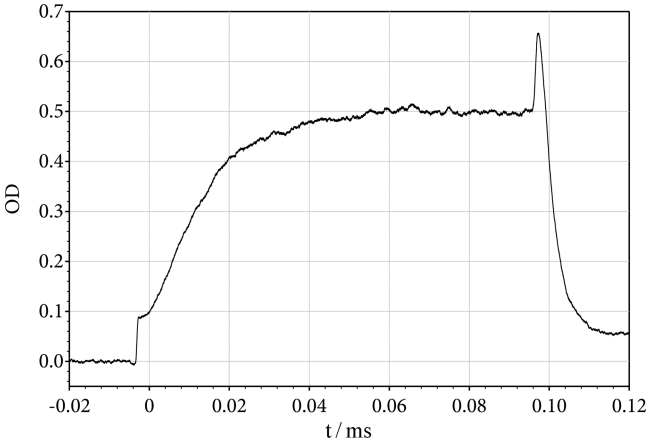

Figure 2. As Figure 1 but behind an incident shock wave (T = 1876 K, [Ar] = 1.4×10^{-5} mol cm^{-3}, $[C_3F_6]_0/[Ar]$ = 520 ppm, dissociation of CF_2 behind reflected shock, see text).

520 ppm of C_3F_6 (one should note that the time scale here is compressed by the density ratio of 3.4 across the shock front; one also notices that CF_2 decomposes behind the reflected shock, in the shown experiment at T = 4030 K and [Ar] = 3.4×10^{-5} mol cm^{-3}, see ref 14).

At lower temperatures, the observation times up to about 1 ms did not suffice to reach the final CF_2 level. Figure 3 shows an example with T = 1568 K, [Ar] = 1.3×10^{-4} mol cm^{-3}, and 530 ppm of C_3F_6. In this case the rate of CF_2 formation could only be evaluated by means of the absorption coefficient ε of CF_2. In order to derive k in eq 6, in addition, here the final level $[CF_2]_{t=\infty}$ had to be reconstructed. We did this be employing the same value for $[CF_2]_{t=\infty}/[C_3F_6]_{t=0}$ as found in higher temperature experiments (1800−2000 K). As we observed no temperature dependence of the CF_2 yield, this procedure did not create uncertainties (we took into account, however, the apparent concentration dependence of the CF_2 yield, see above).

One has to mention one side observation. Apart from the schlieren peaks indicating the arrival of the incident and reflected shock waves at the observation windows, Figures 1−3 show small absorption steps before the dissociation sets in and before CF_2 absorption starts to rise. This absorption step can be attributed to a high-temperature UV absorption of the parent C_3F_6 at 248 nm. While this absorption below about 1000 K is too weak to be

dx.doi.org/10.1021/jp501569a | J. Phys. Chem. A XXXX, XXX, XXX−XXX

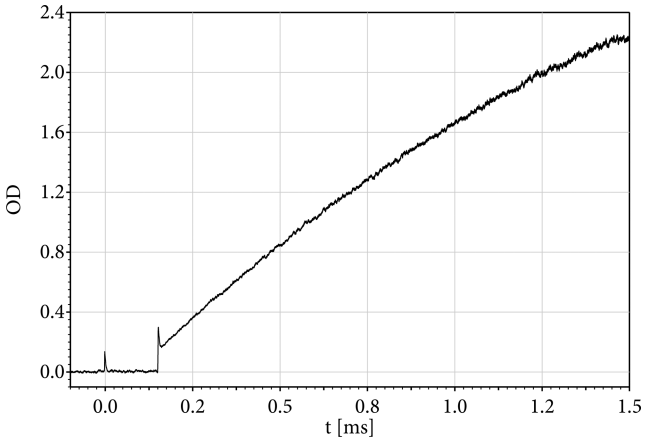

Figure 3. As Figure 1: T = 1568 K, [Ar] = 1.3×10^{-4} mol cm^{-3}, $[C_3F_6]_0$/[Ar] = 520 ppm, absorption step behind schlieren peak due to C_3F_6, see text.

detected,[26,27] with increasing temperature the band with the maximum near 180 nm broadens such that its long-wavelength tail, caused by vibrationally hot molecules, becomes detectable at 248 nm. The temperature dependence of this absorption at 248 nm (with an apparent temperature dependence measured in our work as $\varepsilon \approx 3.2 \times 10^8 \exp(-11\,200\ \mathrm{K}/T)$ cm^2 mol^{-1}, base e) corresponds to expectations,[28] the absolute value at 1500 K being about 1/10 of the maximum value at 180 nm and at room temperature.[26] One accounts for the superimposed absorption of C_3F_6 by shifting the zero line of CF_2 absorption up to the initial absorption step.

The measurement of CF_2 yields contains information on secondary processes following reactions 1−4. For example, C_2F_4 from reaction 4, or from the sequences (1) and (5), under the high-temperature conditions of the present work, decomposes rapidly[16] via

$$C_2F_4(+M) \rightarrow 2CF_2(+M) \qquad \Delta H_0^\circ = 67.5\ \mathrm{kcal\ mol^{-1}} \tag{8}$$

such that a yield of 3 CF_2 per C_3F_6 decomposed arises (the reaction enthalpy at 0 K is from ref 16). However, the participation of reactions 2 and 3 also has to be considered. If reaction 3 would be followed by fast reactions like

$$C_2F_3(+M) \rightarrow CF_2 + CF \qquad \Delta H_0^\circ = 65.9\ \mathrm{kcal\ mol^{-1}} \tag{9}$$

and

$$CF_3 + CF \rightarrow 2CF_2 \qquad \Delta H_0^\circ = -40.4\ \mathrm{kcal\ mol^{-1}} \tag{10}$$

then also a yield of 3 CF_2 per C_3F_6 decomposed would be obtained. However, in this case, because of the bimolecular character of reaction 10, a decrease of the CF_2 yield should be expected at low reactant concentrations. Apparently, we have observed this with our experiments at 60 ppm reactant concentration. Analogous arguments would apply if reaction 2 participates. On the basis of the measured CF_2 profiles alone such conclusions cannot be proven. We come back to this problem later when we have described quantum-chemical and kinetics calculations.

Selected examples for the measured rate constants k in eq 6 and the corresponding experimental conditions are given in Table 1. The table also includes some final CF_2 yields, as far as they could be approached within our observation time. Figure 4 shows rate constants k from experiments with reactant concentrations from about 60 to 1100 ppm in Ar and with [Ar] in the range 2×10^{-6} to 10^{-4} mol cm^{-3}.

Table 1. Examples of Rate Coefficients k (from Eq 6), Experimental Conditions and CF_2 Yields

[Ar]/mol cm^{-3}	$10^6[C_3F_6]_0$/[Ar]	T/K	k/s^{-1}	$[CF_2]_\infty/[C_3F_6]_0$
2.7×10^{-6}	1100	1895	1.2×10^4	2.7
2.6×10^{-6}	1100	1939	1.7×10^4	2.3
2.3×10^{-6}	1100	2117	5.9×10^4	2.4
2.1×10^{-6}	1100	2211	5.9×10^4	2.3
9.2×10^{-5}	530	1330	4.1×10^0	–
9.0×10^{-5}	530	1343	5.8×10^0	–
8.8×10^{-5}	530	1336	2.6×10^0	–
7.9×10^{-5}	530	1464	4.1×10^1	–
7.6×10^{-5}	530	1496	1.3×10^2	–
7.0×10^{-5}	530	1616	1.1×10^3	–
6.7×10^{-5}	530	1726	4.0×10^3	2.6
6.3×10^{-5}	530	1753	7.3×10^3	2.6
6.4×10^{-5}	530	1810	1.3×10^4	2.6
2.0×10^{-5}	82	1720	4.3×10^3	2.1
2.0×10^{-5}	82	1854	1.3×10^4	1.9
1.9×10^{-5}	82	1915	2.1×10^4	1.7
6.9×10^{-5}	75	1843	1.4×10^4	1.8
6.5×10^{-5}	75	1900	3.2×10^4	1.6
6.2×10^{-5}	75	2011	9.6×10^4	–
5.9×10^{-5}	75	2086	8.7×10^4	–
9.5×10^{-5}	63	1504	6.0×10^1	–
9.1×10^{-5}	63	1538	1.1×10^2	–
8.2×10^{-5}	63	1634	3.7×10^2	–
7.3×10^{-5}	63	1773	6.9×10^3	1.8
6.4×10^{-5}	63	1978	3.5×10^4	–

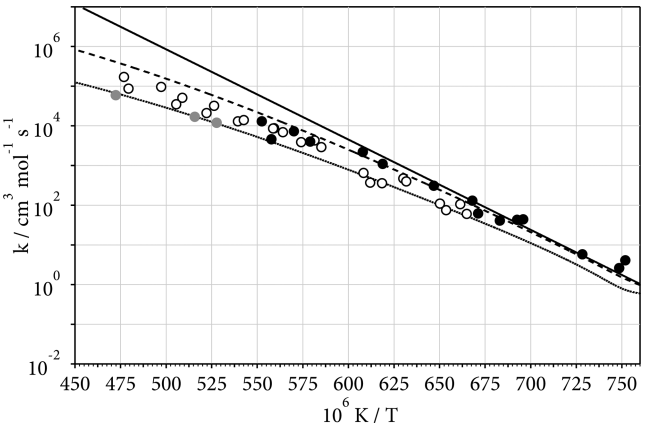

Figure 4. Rate constants k of the dissociation of C_3F_6 (curves from top to bottom: modeled k_∞ from eq 13, k([Ar] = 7×10^{-5} mol cm^{-3}), and k([Ar] = 3×10^{-6} mol cm^{-3}); experimental results for $[C_3F_6]_0$/[Ar] ≈ 500 pm (○) and 70 ppm (●) and [Ar] = (2−10) × 10^{-5} mol cm^{-3}; experimental results for [Ar] = (2−3) × 10^{-6} mol cm^{-3}).

We did not observe a dependence of the apparent rate constants on the reactant concentration. However, with decreasing bath gas concentration [Ar], a significant decrease of k was observed. Near 2000 K this was about a factor of 4 when [Ar] was lowered from 8×10^{-5} to 2×10^{-6} mol cm^{-3}. This decrease later on will be attributed to falloff effects of the unimolecular reaction and analyzed accordingly. Using only experiments with [Ar] ≈ 8×10^{-5} mol cm^{-3}, an apparent rate constant of

$$k = 8.3 \times 10^{13} \exp(-40890\ \mathrm{K}/T)\ \mathrm{s^{-1}} = 8.3 \times 10^{13} \exp(-81.3\ \mathrm{kcal\ mol^{-1}}/RT)\ \mathrm{s^{-1}} \tag{11}$$

dx.doi.org/10.1021/jp501569a | J. Phys. Chem. A XXXX, XXX, XXX−XXX

would be obtained, giving 3.6 s^{-1} at 1330 K and 10^5 s^{-1} at 2000 K. We emphasize that this apparent rate constant corresponds to the falloff range and needs further analysis such as given below.

3. QUANTUM-CHEMICAL AND KINETIC MODELING OF PRIMARY DISSOCIATION PATHWAYS

As in our previous work,[16,17] quantum-chemical calculations of the energy profiles of possible primary dissociations and kinetic modeling by unimolecular rate theory help to understand the observations. A variety of ab initio methods were employed to characterize the energetics, while DFT calculations were used to determine transition-state vibrational frequencies and rotational constants for reaction 9; see Appendix. Table 2 shows reaction

Table 2. Calculated Reaction Enthalpies and Enthalpies of Transition States (at 0 K, in kcal mol^{-1}, See Text)

reaction	CBS-QB3[29]	G4MP2[31]	G4[30]
$C_3F_6 \rightarrow CF_3CF + CF_2$ (1)	106.4	102.3	104.1
$C_3F_6 \rightarrow CF_3 + C_2F_3$ (3)	110.5	105.0	107.0
$C_3F_6 \rightarrow CF_2CF_2CF_2^{\ddagger}$(TS1)	86.5	84.8	84.9
$CF_2CF_2CF_2^{\ddagger}$(TS1) $\rightarrow CF_2CF_2CF_2$	−31.7	19.5	18.6
$CF_2CF_2CF_2 \rightarrow C_2F_4{-}CF_2^{\ddagger}$(TS2)	19.5	19.5	18.6
$C_2F_4{-}CF_2^{\ddagger}$(TS2) $\rightarrow C_2F_4 + CF_2$	−6.5	−7.7	−7.0
$C_2F_3 \rightarrow CF + CF_2$ (9)	65.7	63.3	64.6

enthalpies obtained from CBS-QB3,[29] G4,[30] and G4MP2[31] calculations using the Gaussian 09 software.[32]

Enthalpies for the transition state of reaction 4 and the secondary dissociation (9) are also given. Figure 5 compares the energetics of the competing primary pathways. While reactions 1−3 are simple bond fissions with loose activated complexes, reaction 4 has to overcome an activation barrier and involves an intrinsically more complicated mechanism.

This is specifically shown by its energy diagram as obtained from G4 calculations in Figure 6. Details of our quantum-chemical calculations are provided in the Appendix.

Several differing energy profiles for reaction 4 have been proposed before[19,20,25] (see their discussion in ref 5). Our calculations favor ref 19 over ref 20, with TS1 being markedly above TS2. On the other hand, pathways from C_3F_6 to CF_2 + C_2F_4 passing through c-C_3F_6 were described in ref 25 while Figure 6 shows a pathway passing through $CF_2CF_2CF_2$. Likewise, our calculations in part II[24] showed a pathway from c-C_3F_6 to CF_2 + C_2F_4 passing through $CF_2CF_2CF_2$, whereas a direct, single-transition state pathway from c-C_3F_6 to CF_2 + C_2F_4 was proposed in ref 25. These details of the multidimensional potential energy surface are of importance when rates of forward and backward reactions are compared, see below and part II. We also inspected whether reactions 1 and 3 really are simple bond fissions. This is confirmed by the Morse-type energy profiles of these two reactions shown in Figure 7. A Morse-type energy profile between the central C and F atoms was also obtained in ref 33 for reaction 2. As this reaction is energetically higher than reactions 1 and 3 and is entropically less favored, this reaction presumably is only of minor importance in thermal dissociation experiments, see below.

Theoretical modeling of the rate constants k_1−k_4 is difficult for a number of reasons. First, this is a four-channel unimolecular reaction system for which, at pressures below the high-pressure limit, the contribution of the energetically higher reaction channels in comparison to single-channel unimolecular reactions

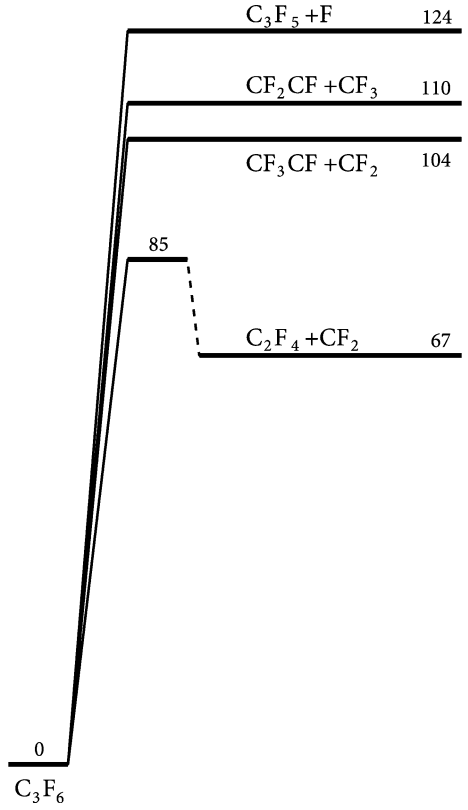

Figure 5. Energetics of the primary dissociation channels of C_3F_6 dissociation (results of G4 calculations[30]).

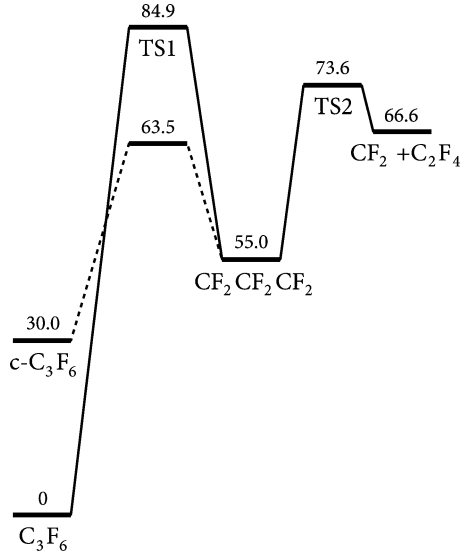

Figure 6. Energetics of reactions 4, 14, and 15 (results of G4 calculations[30]).

is reduced, see ref 34. In the present work this effect could not yet be handled and reactions 1−4 were treated as single-channel reactions. Second, the reactions 1−4 under the present high-temperature conditions are expected to be in the falloff range such that high pressure (k_∞), low pressure (k_0), and intermediate falloff rate constants need to be characterized. The high-pressure rate constant for reaction 4, $k_{4,\infty}$, was estimated by transition-state theory with the molecular parameters given in the Appendix. We obtained $k_{4,\infty} \approx 4.1 \times 10^{13} \exp(-86.7 \text{ kcal mol}^{-1}/RT)$ s^{-1}, i.e., $k_{4,\infty}(2000\text{ K}) \approx 1.4 \times 10^4$ s^{-1} and $k_{4,\infty}(1330\text{ K}) \approx 0.023$ s^{-1}.

dx.doi.org/10.1021/jp501569a | J. Phys. Chem. A XXXX, XXX, XXX−XXX

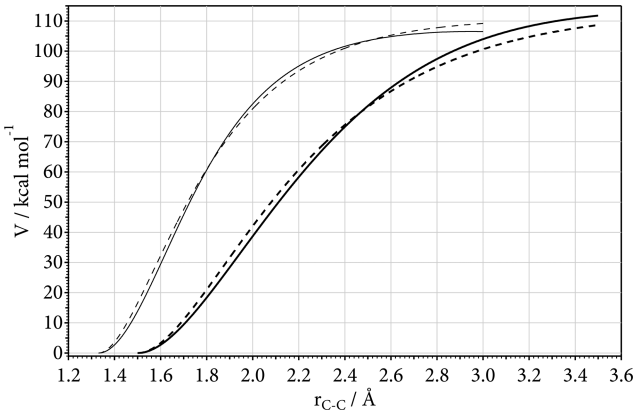

Figure 7. MEP energies for reaction 1 (upper curves: dashed line Morse potential with D_e = 111 kcal mol^{-1} and β = 2.87 Å^{-1}; solid line $\beta(r)$/Å^{-1} = 2.32 + 1.59(r − 1.33 Å) − 0.95(r − 1.33 Å)^2) and for reaction 3 (lower curves: dashed line D_e = 114 kcal mol^{-1}, β = 1.87 Å^{-1}; solid line $\beta(r)$/Å^{-1} = 1.67 + 0.10(r − 1.5 Å) + 0.11(r − 1.5 Å)^2) from CBS-QB3 calculations.[29]

Taking into consideration that falloff effects further reduce k_4 to values below $k_{4,\infty}$, by comparison with the experiments we conclude that this reaction is too slow to contribute to k to a major extent under the present conditions. However, this pathway may become more important for lower temperatures and pressures; see below and the examples of ref 17. A calculation of $k_{1,\infty}$, $k_{2,\infty}$, and $k_{3,\infty}$ (similar to $k_{8,\infty}$ in ref 18) requires more detailed information on the potential energy surface than was available here. Therefore, only a preliminary attempt was made to estimate these rate constants with the simplified version of the statistical adiabatic channel model (SACM/CT) from refs 36 and 37. In doing this, the potential was characterized by the standard value α/β = 0.5 of the ratio of its anisotropy parameter α and its Morse parameter β, see ref 36. We are aware of the limitations of this approach and, therefore, allow for a fine-tuning of the results after comparison with the experiments. With α/β = 0.5, we obtained $k_{1,\infty} \approx 1.3 \times 10^{16} \exp(-97 \text{ kcal mol}^{-1}/RT)$ s^{-1}, $k_{2,\infty} \approx 1.4 \times 10^{16} \exp(-119 \text{ kcal mol}^{-1}/RT)$ s^{-1}, and $k_{3,\infty} \approx 3.0 \times 10^{15} \exp(-101 \text{ kcal mol}^{-1}/RT)$ s^{-1} (derived between 1500 and 2000 K). This would correspond to branching fractions of $k_{1,\infty}$:$k_{2,\infty}$:$k_{3,\infty} \approx$ 0.94:0.007:0.059 at 1500 K and 0.92:0.004:0.077 at 2000 K. These results suggest that reaction 2 , for energetic and entropic reasons, only plays a minor role. In the following, therefore, we try to rationalize our observations in terms of reactions 1 and 3 only. Comparing the modeled $k_{1,\infty}$ + $k_{3,\infty}$ with the measured values of k from eq 11, we find close agreement near 1400 K, but smaller values by a factor of 3.5 near 2000 K. However, we emphasize that falloff effects have to be taken in account such as elaborated below which changes the comparison.

We mention that the dissociation channels (1) and (3) were the only ones included in the modeling of the more complex reaction mechanisms studied in refs 11−13. Here, values of $k_1 = 10^{13.0} \exp(-78.4 \text{ kcal mol}^{-1}/RT)$ s^{-1} and $k_3 = 10^{16.7} \exp(-104.9 \text{ kcal mol}^{-1}/RT)$ s^{-1} were employed. The sum of k_1 + k_3 of these fitted values is not far from our measurements of k from eq 11, k_1 + k_3 being 2.0 × 10^5 s^{-1} at 2000 K and 1.6 × 10^{-1} s^{-1} at 1330 K. However, this near agreement needs further discussion. In particular, the low preexponential factor and the large difference between the apparent activation energy of k_1 and the bond energy raise doubts about this rate constant. As the single-pulse shock wave experiments from ref 11 were done at similar temperatures and pressures as the present experiments, nevertheless, the results for k should be comparable with the present work. However, branching fractions k_1/k and k_3/k from ref 11, because of the given arguments, appear doubtful.

The experimental apparent activation energy of 81.3 kcal mol^{-1} for k from eq 11 is significantly below the modeled values for $k_{1,\infty}$ of 97 kcal mol^{-1} and for $k_{3,\infty}$ of 101 kcal mol^{-1}. We explain this by stronger falloff of k_1 below $k_{1,\infty}$ (and of k_3 below $k_{3,\infty}$) at higher temperatures than at lower temperatures. In order to estimate the magnitude of $k_1/k_{1,\infty}$ (and $k_3/k_{3,\infty}$), we modeled full falloff curves by the methods of refs 35−40. First, we modeled single-channel limiting low-pressure rate constants $k_{1,0}$ and $k_{3,0}$ using molecular parameters as given in the Appendix. Over the temperature range 1500−2000 K, we obtained $k_{1,0} \approx [\text{Ar}]\ 3.8 \times 10^{25} (T/1500 \text{ K})^{-16.7} \exp(-104 \text{ kcal mol}^{-1}/RT)$ cm^3 mol^{-1} s^{-1}, and $k_{3,0} \approx [\text{Ar}]\ 1.8 \times 10^{26} (T/1500 \text{ K})^{-17.5} \exp(-109.8 \text{ kcal mol}^{-1}/RT)$ cm^3 mol^{-1} s^{-1}. Second, following refs 39 and 40 we estimated the center broadening factors F_{cent} of the falloff curves as $F_{cent,1} \approx 0.025$ and $F_{cent,3} \approx 0.024$. For such small values of F_{cent}, the representation of "broad" falloff curves from ref 38 appears most adequate, i.e., $k/k_\infty = [\ x/(1+x)]F(\ x)$ with $x = k_0/k_\infty$ and

$$F(x) \approx (1+x)/[1+x^n]^{1/n} \quad (12)$$

where $n = [\ln 2/\ln(2/F_{cent})]\ [0.8 + 0.2x^q]$ and $q = (F_{cent} - 1)/\ln(F_{cent}/10)$. Inserting k_0 and k_∞ as given above for reactions 1 and 3, for an average bath gas concentration of [Ar] ≈ 8 × 10^{-5} mol cm^{-3}, one obtains $k/k_\infty \approx 0.82$ at 1500 K and 0.33 at 2000 K. Correcting k from eq 11 for falloff effects in k_1 and k_3 then leads to

$$k_\infty \approx 2 \times 10^{17} \exp(-104 \text{ kcal mol}^{-1}/RT) \text{ s}^{-1} \quad (13)$$

This result is close to our modeled k_∞ = $k_{1,\infty}$ + $k_{3,\infty}$ given above. The decrease of k with decreasing [Ar] is much more pronounced at higher than at lower temperatures. We illustrate this effect by including in Figure 4 modeled apparent rate constants k for constant [Ar] = 3 × 10^{-6} and 7 × 10^{-5} mol cm^{-3}. The modeled results agree well with our measurements (over the range 1900−2200 K). Falloff effects become less important with decreasing temperature; they would almost have disappeared near 1400 K for our range of [Ar]. Figure 8 illustrates this behavior by examples of falloff curves for k_1([Ar],T).

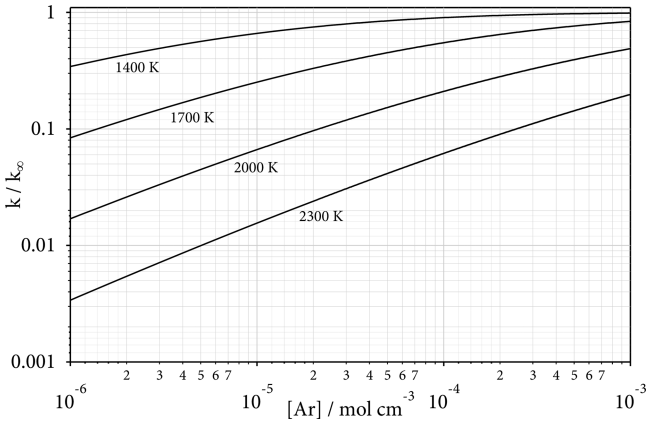

Figure 8. Modeled falloff curves for C_3F_6 dissociation at T = 1400, 1700, 2000, and 2300 K (from top to bottom, eq 12 with k_∞ from eq 13, $k_0 \approx$ [Ar] 4 × 10^{23} (T/1500 K)$^{16.7}$ exp(−104 kcal mol^{-1}/RT) cm^3 mol^{-1} s^{-1}, and $F_{cent} \approx 0.025$).

We note that $k_{1,\infty} \approx 2k_\infty/3$ from eq 13 is satisfactorily close to the modeled $k_{1,\infty}$ given above while $k_{3,\infty} \approx k_\infty/3$ from eq 13 is smaller than the modeled value. However, the assumption of

dx.doi.org/10.1021/jp501569a | J. Phys. Chem. A XXXX, XXX, XXX−XXX

$\alpha/\beta \approx 0.5$ need not to be fulfilled for all cases; it just represents a first guess to be modified by experiment. We finally estimate below which temperature the rigid activated complex process (4) will dominate over the bond fission processes (1) + (3) (only high-pressure rate constants need to be considered). We find that reaction 4 will dominate over reactions 1 and 3 only at temperatures below about 1100 K, when k is smaller than about 4×10^{-4} s^{-1}. Reaction 4 according to Figure 6 may then lead to $C_2F_4 + CF_2$ via TS2 or, after intermediate formation of c-C_3F_6, by fast subsequent dissociation of the latter molecule (see part II).

4. SECONDARY REACTIONS AND BRANCHING FRACTIONS

So far we assumed that the observed drop of the CF_2 yield from about 3 to 2 per decomposed C_3F_6 with decreasing reactant concentration was explainable by a change from a mechanism with the reactions

$$C_3F_6 \rightarrow CF_3CF + CF_2 \quad (1)$$

$$CF_3CF \rightarrow C_2F_4 \quad (5)$$

$$C_2F_4 \rightarrow 2CF_2 \quad (8)$$

and

$$C_3F_6 \rightarrow C_2F_3 + CF_3 \quad (3)$$

$$C_2F_3 \rightarrow CF_2 + CF \quad (9)$$

$$CF_3 + CF \rightarrow 2CF_2 \quad (10)$$

to a mechanism of reactions 1, 5, and 8 only. In order to quantify this assumption, we first assumed that the rate of reaction 9 is similar to that of the nearly isoenergetic dissociation (8), both reactions being faster than reaction 1. We further estimated that k_{10} is of the order of $10^{12}-10^{13}$ cm^3 mol^{-1} s^{-1} (values obtained by SACM/CT calculated with $\alpha/\beta \approx 0.5$, see above, and similar values for the reactions $CF_3 + CF_3 \rightarrow C_2F_6$ or $CF_2 + CF_2 \rightarrow C_2F_5$). With these values, reaction 10, for reactant concentrations below 100 ppm, becomes too slow to generate CF_2 on our observation time such that the observed CF_2 yield drops from 3 to 2 per parent molecule. The corresponding CF_2 yields thus reflect the ratio of k_1 and k_3 as employed above. The measured CF_2 yields are slightly below 3 and 2, for high and low reactant concentrations, respectively. This could be due to minor contributions from reaction 2, or due to uncertainties in the absorption coefficient ε of CF_2 (estimated uncertainty 10%), or due to other experimental problems. We are unable to decide between these three possibilities.

We finally discuss possibilities for the formation of C_3F_6 from CF_2 and C_2F_4. We consider two pathways: first, the reverse of reaction 4 and, second, a mechanism involving the reverse of reactions 1 and 5, both described by the overall reaction

$$CF_2 + C_2F_4 \rightarrow C_3F_6 \quad (14)$$

Reaction 14 has to be considered in comparison to the alternative formation of c-C_3F_6, i.e.

$$CF_2 + C_2F_4 \rightarrow \text{c-}C_3F_6 \quad (15)$$

Combining the equilibrium constant $K_{c,4} = [CF_2][C_2F_4]/[C_3F_6]$ from ref 4, $K_{c,4} = 1.93 \times 10^2 \exp(-61.6 \text{ kcal mol}^{-1}/RT)$ mol cm^{-3}, with our modeled $k_{4,\infty} = 4.1 \times 10^{13} \exp(-86.7 \text{ kcal mol}^{-1}/RT)$ s^{-1} leads to $k_{14,a} = k_{4,\infty}/K_{c,4}$ of

$$k_{14,a} \approx 2.1 \times 10^{11} \exp(-25.1 \text{ kcal mol}^{-1}/RT) \text{ cm}^3 \text{ mol}^{-1} \text{ s}^{-1} \quad (16)$$

for the reverse of reaction 4. The reverse of reaction 5, followed by the reverse of reaction 1, on the other hand, leads to a rate constant $k_{14,b} = k_{1,\infty}/K_{c,4}$ which with our measured $k_{1,\infty} = 1.3 \times 10^{17}$ $\exp(-104 \text{ kcal mol}^{-1}/RT)$ s^{-1} is given by

$$k_{14,b} \approx 6.9 \times 10^{14} \exp(-42.4 \text{ kcal mol}^{-1}/RT) \text{ cm}^3 \text{ mol}^{-1} \text{ s}^{-1} \quad (17)$$

In both cases, falloff corrections would have to be applied at high temperatures. Analogous to the dissociation pathways, $k_{14,a}$ would be larger than $k_{14,b}$ at temperatures below about 1100 K. On the other hand, $k_{14} = k_{14,a} + k_{14,b}$ is always much smaller than $k_{15} = 1.9 \times 10^{10} \exp(-7.8 \text{ kcal mol}^{-1}/RT)$ cm^3 mol^{-1} s^{-1} from part II. Nevertheless, as long as the formation of c-C_3F_6 by reaction 15 is immediately followed by dissociation, reaction 14 with $k_{14} = k_{14,a} + k_{14,b}$ may lead to the formation C_3F_6 from $CF_2 + C_2F_4$. Estimates of k_{14} from a modeling of a more complex mechanism in refs 41 and 42 near 1500 K agree with the present $k_{14,b}$, while estimates of k_{14} from ref 43 near 1000 K overestimate $k_{14,a}$ by about a factor of 20. This confirms an inconsistency noted before in ref 5.

5. CONCLUSIONS

The present article describes measurements of CF_2 formation in the thermal decomposition of C_3F_6. The reaction in the temperature range 1330−2210 K was shown to be in the falloff range of the unimolecular reaction. The simple bond fissions

$$CF_3—CF=CF_2 \rightarrow CF_3—CF + CF_2 \quad (1)$$

$$CF_3—CF=CF_2 \rightarrow CF_3 + CF=CF_2 \quad (3)$$

were found to dominate over the rigid activated complex process

$$C_3F_6 \rightarrow CF_2CF_2CF_2 \rightarrow C_2F_4 + CF_2 \quad (4)$$

at temperatures above about 1100 K. Under these conditions, the thermal dissociations of C_3F_6 and c-C_3F_6 (the latter described in part II and passing over the same $CF_2CF_2CF_2$ biradical) thus apparently do not involve the same intermediate. The branching between reactions 1 and 3 and subsequent secondary reactions determine the final CF_2 yields which were found to be between about 2 and 3 CF_2 per parent C_3F_6 decomposed. Primary branching fractions CF_2:CF_3 were found to be about 0.67:0.33 in fair agreement with the values 0.8:0.2 from IR multiphoton dissociation experiments.[2] Falloff effects of the primary dissociations, which were not taken into account in previous work, have been quantified in terms of low-pressure and high-pressure rate constants and center broadening factors of the falloff curve. For example, $k_{1,0} \approx [\text{Ar}]3.8 \times 10^{25}(T/1500 \text{ K})^{-16.7} \exp(-104$ kcal mol$^{-1}/RT$) cm^3 mol^{-1} s^{-1}, $k_{1,\infty} \approx 1.3 \times 10^{17} \exp(-104$ kcal mol$^{-1}/RT$) s^{-1}, and $F_{\text{cent},1} \approx 0.025$ were proposed for the dominant primary dissociation channel (1), eq 12 describing the full falloff curve.

APPENDIX

Molecular Parameters Used in Modeling

(a). Harmonic Vibrational Frequencies. C_3F_6. ν_i/cm^{-1} = 31, 122, 177, 239, 248, 357, 364, 458, 506, 565, 595, 650, 652, 761, 1037, 1169, 1209, 1218, 1331, 1383, 1814 from B3LYP/6-31G(2df,p) calculations scaled by 0.9854 (from G4 model); ν_i/cm^{-1} = 120, 120, 180, 237, 251, 359, 368, 456, 505, 550, 597, 637, 765, 1047, 1201, 1231, 1238, 1356, 1415, 1851 from ref 4.

dx.doi.org/10.1021/jp501569a | J. Phys. Chem. A XXXX, XXX, XXX−XXX

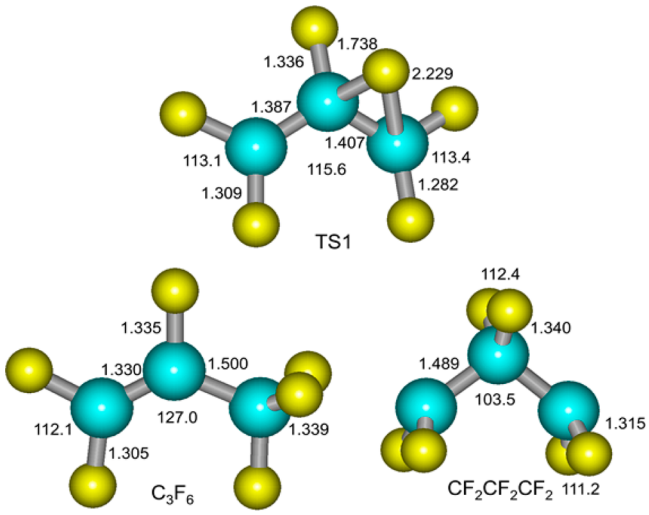

Figure 9. Optimized structures of C_3F_6, upper TS1, and $CF_2CF_2CF_2$ (from B3LYP/6-31G(2df) calculations of the present work; bond lengths in Å, bond angles in deg).

$C_3F_6 \rightarrow CF_2 + C_2F_4$. Transition state TS1: ν_i/cm^{-1} = 82, 118, 158, 192, 254, 300, 369, 395, 420, 457, 532, 566, 604, 737, 1070, 1205, 1353, 1461, 1568, 1586, and 457i from B3LYP/6-31G(2df,p) calculations scaled by 0.9854 (G4 model).

(b). Rotational Constants. C_3F_6. *A*, *B*, and C/cm^{-1} = 0.085, 0.042, and 0.033 from B3LYP/6-31G(2df,p) calculations (G4 model); 0.184, 0.110, and 0.0687 from ref 4.

$C_3F_6 \rightarrow CF_2 + C_2F_4$. Transition state TS1: *A*, *B*, and C/cm^{-1} = 0.073, 0.046, and 0.036 from B3LYP/6-31G(2df,p) calculations (G4 model).

(c). Enthalpies of Formation (at 0 K and in kcal mol^{-1}). F 18.47 (ref 4); CF 58.16 (ref 4); $^1CF_2$ −46.6 (refs 4 and 16); CF_3 −111.0 (ref 4); C_2F_3 −54.3 (ref 4); C_2F_4 −160.6 (ref 4); CF_3CF ≈−144 (refs 1, 4, and 16), ≈−124.4 (G4 from this work); CF_3CFCF ≈−172 (refs 1 and 4), ≈−169.4 (G4 from this work); C_3F_6 −275.1 (ref 4); c-C_3F_6 ≈−243.8 (G4 from this work).

(d). Details of Quantum-Chemical Calculations. In the main composite method employed here, the G4 calculations, the equilibrium geometry of the considered species was estimated at the B3LYP/6-31G(2df, p) level. Afterward, a series of single-point energies were calculated by using Hartree−Fock and post-Hartree−Fock molecular orbital methods with different basis sets. Finally, the following combined expression was used to estimate the energy at 0 K: $E_0(G4) = E[MP4/6\text{-}31G(d)] + E[MP4/6\text{-}31+G(d) - MP4/6\text{-}31G(d)] + E[MP4/6\text{-}31G(2df,p) - MP4/6\text{-}31G(d)] + E[CCSD(T)/6\text{-}31G(d) - MP4/6\text{-}31G(d)] + E[MP2(full)/G3LargeXP - MP2/6\text{-}31G(2df, p) - MP2/6\text{-}31+G(d) + MP2/6\text{-}31G(d)] + E[HF/limit - HF/G3LargeXP] + E(SO) + E(HLC) + E(ZPE)$

Here HF/limit denotes the Hartee−Fock energy limit, *E*(SO) is the spin−orbit correction for the atoms, *E*(HLC) is the high-level correction term, and *E*(ZPE) the zero-point energy correction computed with the B3LYP/6-31G(2df,p) harmonic vibrational frequencies scaled by 0.9854. Normally, the computed values of E_0(G4) approach well those obtained at the CCSD(T) level while an extrapolated complete basis set with a strong reduction of the computational resources is possible. The average deviation of the G4 results from experimental enthalpies of formation was found to be about 0.8 kcal mol^{-1}.

The structures of the two transition states TS1 and TS2, and of the intermediate singlet biradical $CF_2CF_2CF_2$, as obtained from B3LYP/6-31G(2df) calculations are illustrated in Figures 9−11. f10 Intrinsic reaction coordinate calculations were made, showing that the three structures indeed are linked by smooth pathways.

In order to classify whether the G4 method is appropriate for computing the energy of the singlet $CF_2CF_2CF_2$ biradical, multiconfigurational effects were investigated by CCSD/6-311+G(d) calculations. The resulting T1 value of 0.018 indicated that nondynamical effects for the biradical are expected to be insignificant (see ref 44). To support this conclusion, a comparison between the CASPT2(6/6)/6-311+G(2df,2p) results from ref 23 (with a small active space of 6 electrons and 6 orbitals) and the present G4 calculations (essentially CCSD(T,full)/CBS) was carried out. The energy for ring opening of c-C_3F_6 to $CF_2CF_2CF_2$ in ref 23 at 423 K was found

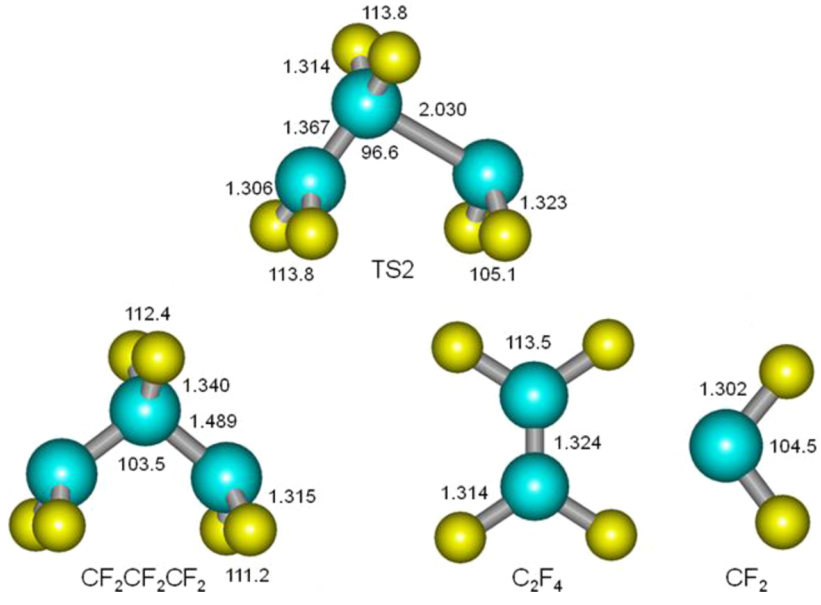

Figure 10. As Figure 9, for $CF_2CF_2CF_2$, TS2, and $C_2F_4 + CF_2$.

dx.doi.org/10.1021/jp501569a | J. Phys. Chem. A XXXX, XXX, XXX−XXX

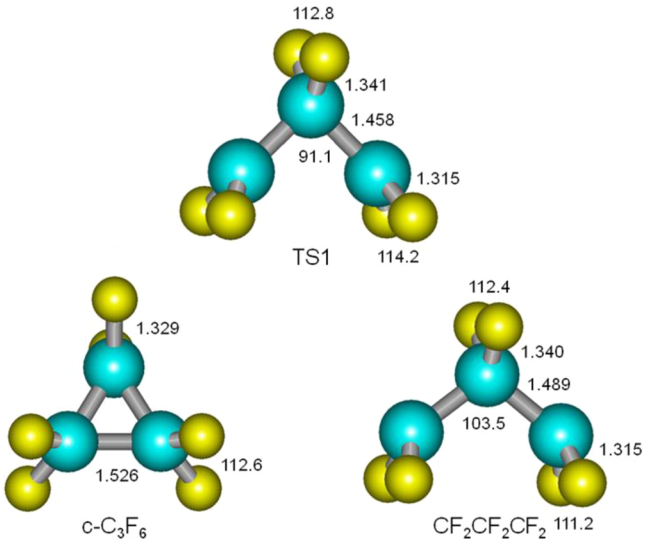

Figure 11. As Figure 9, for c-C_3F_6, lower TS1, and $CF_2CF_2CF_2$.

to be 30.5 kcal mol^{-1} while our G4 value was 33.5 kcal mol^{-1}. The electronic barrier for the reverse process of 9.8 kcal mol^{-1} from the CASPT2 calculations compares with 8.5 kcal mol^{-1} from the G4 calculations. The activation barrier for the complete process c-C_3F_6 → TS_2 → C_2F_4 + CF_2 of 42.0 kcal mol^{-1} from CASPT/2 compares well with the present G4 value of 43.6 kcal mol^{-1}. Neglecting minor temperature effects, this agreement suggests that nondynamical correlation effects here are insignificant.

■ AUTHOR INFORMATION

Corresponding Author

*E-mail: shoff@gwdg.de. Tel.: +49-(0)551-3933112.

Notes

The authors declare no competing financial interest.

■ ACKNOWLEDGMENTS

Support of this work by K. Hintzer and A. Thaler is gratefully acknowledged.

■ REFERENCES

(1) Longfellow, C. A.; Smoliar, L. A.; Lee, Y. T.; Yeh, C. Y.; Lin, S. M. The Photodissociation Dynamics of Hexafluoropropene Examined at 193 nm. *Chem. Phys. Lett.* **1997**, *271*, 33−39.

(2) Longfellow, C. A.; Smoliar, L. A.; Lee, Y. T.; Lee, Y. R.; Yeh, C. Y.; Lin, S. M. Competing Pathways in the Infrared Multiphoton Dissociation of Hexafluoropropene. *J. Phys. Chem. A* **1997**, *101*, 338−344.

(3) Rubio, L.; Santos, M.; Torresano, J. A. Laser Induced Fluorescence Detection of CF, CF_2, and CF_3 in the Infrared Multiphoton Dissociation of C_3F_6. *J. Photochem. Photobiol. A: Chem.* **2001**, *146*, 1−8.

(4) Goos, E.; Burcat, B. Extended Third Millenium Ideal Gas and Condences Phase Thermochemical Data Base for Combustion with Updates from Active Thermochemical Tables; ftp.technion.ac.il/pub/supported/aetdd/thremodynamics; July 2013.

(5) Poutsma, M. L. Chain Elongation during Thermolysis of Tetrafluoroethylene and Hexafluoropropylene: Modeling of Mechanistic Hypotheses and Elucidation of Data Needs. *J. Anal. Appl. Pyrol.* **2011**, *92*, 25−42.

(6) Bacskay, G. B. Quantum Chemical Characterization of the Ground and Excited Singlet and Triplet States of CH_3CF and CF_3 and their Photochemical Isomerization and Dissociation Pathways. *Mol. Phys.* **2003**, *101*, 1955−1965.

(7) Matula, R. A. The Thermal Decomposition of Perfluoropropene. *J. Phys. Chem.* **1968**, *72*, 3054−3056.

(8) Bauer, S. H.; Hou, K. C.; Resler, E. L. Single Pulse Shock Tube Studies of the Pyrolysis of Fluorocarbons and of the Oxidation of Perfluoroethylene. *Phys. Fluids Suppl. I* **1969**, 125−132.

(9) Bauer, S. H.; Javanovic, S. The Pyrolysis of Octafluorocyclobutane − Revisited. *Int. J. Chem. Kinet.* **1998**, *30*, 171−177.

(10) Buravtsev, N. N.; Grigor'ev, A. S.; Kolbanovskii, Y. A. Kinetics and Mechanism of Pyrolysis of Hexafluorocarbene. *Kinet. Catal.* **1989**, *30*, 21−30.

(11) Hynes, R. G.; Mackie, J. C.; Masri, A. R. Shock Tube Study of the Pyrolysis of the Halon Replacement Molecule CF_3CHFCF_3. *J. Phys. Chem. A* **1999**, *103*, 54−61.

(12) Hynes, R. G.; Mackie, J. C.; Masri, A. R. Shock Tube Study of the Oxidation of C_3F_6 by N_2O. *J. Phys. Chem. A* **1999**, *103*, 5967−5977.

(13) Hynes, R. G.; Mackie, J. C.; Masri, A. R. A Shock Tube Kinetics Study on the Reaction of C_3F_6 and H Atoms at High Temperatures. *Proc. Combust. Inst.* **2000**, *28*, 1557−1562.

(14) Cobos, C. J.; Croce, A. E.; Luther, K.; Troe, J. Shock Wave Study of the Thermal Decomposition of CF_3 and CF_2 Radicals. *J. Phys. Chem. A* **2010**, *114*, 4755−4761.

(15) Cobos, C. J.; Croce, A. E.; Luther, K.; Troe, J. Experimental and Modelling Study of the Unimolecular Thermal Decomposition of CHF_3. *Z. Phys. Chem.* **2011**, *225*, 1019−1028.

(16) Cobos, C. J.; Croce, A. E.; Luther, K.; Sölter, L.; Tellbach, E.; Troe, J. Experimental and Modeling Study of the Reaction C_2F_4 (+ M) ⇔ CF_2 + CF_2 (+ M). *J. Phys. Chem. A* **2013**, *117*, 11420−11429.

(17) Cobos, C. J.; Sölter, L.; Tellbach, E.; Troe, J. Shock Wave and Modeling Study of the Thermal Decomposition Reactions of Pentafluoroethane and 2-H-Heptafluoropropane. *Phys. Chem. Chem. Phys.* **2014**, *16*, 9797−9807.

(18) Cobos, C. J.; Croce, A. E.; Luther, K.; Troe, J. Temperature and Pressure Dependence of the Reaction 2 CF_3 (+ M) ⇔ C_2F_6 (+ M). *J. Phys. Chem. A* **2010**, *114*, 4748−4754.

(19) Bilera, I. V.; Borisov, Y. A.; Buravtsev, N. N.; Kolbanovskii, Y. A. Thermal Gas Phase Reactions in the 3C and 6F System: New Spectral, Kinetic, and Quantum- Chemical Data. *Dokl. Phys. Chem.* **2003**, *388*, 63−66.

(20) Kohler, W. H.; Ritter, E. R. Pathways to Perfluoropropene: An MCSCF Inverstigation. Chemical and Physical Processes in Combustion (Combustion Institute, Eastern Section US, Fall Technical Meeting, 2001; p 107, results shown in ref 5.

(21) Buravtsev, N. N.; Kolbanovskii, Y. A. Intermediates of Thermal Transformations of Perfluoro-Organic Compounds. New Spectral Data and Reactions. *J. Fluorine Chem.* **1999**, *96*, 35−42.

(22) Buravtsev, N. N.; Kolbanovskii, Y. A. Mechanism of Hexafluoropropylene Formation in the Gas-Phase Pyrolysis of Tetrafluoroethylene. *Russ. J. Appl. Chem.* **2002**, *75*, 598−605.

(23) Wei, H.; Hrovat, D. A.; Dolbier, W. R.; Smart, B. E.; Borden, W. T. The "Bond-Stretched Invertomer" of Hexafluorocyclopropane—a New Type of Reactive Intermediate. *Angew.Chem. Int. Ed.* **2007**, *46*, 2666−2668.

(24) Cobos, C. J.; Sölter, K.; Tellbach, E.; Troe, J. Shock Wave Study of the Thermal Dissociations of C_3F_6 and c-C_3F_6. II. Dissociation of Hexafluorocyclopropane and Dimerization of CF_2. *J. Phys. Chem. A* **2014**, DOI: 10.1021/jp501577k.

(25) Yu, H.; Kennedy, E. M.; Ong, W.-H.; Mackie, J. C.; Han, W.; Dlugogorski, B. Z. Experimental and Kinetic Studies of the Gas-Phase Pyrolysis of n-C_4F_{10}. *Ind. Eng. Chem. Res.* **2008**, *47*, 2579−2584.

(26) Sharpe, S.; Hartnett, B.; Sethi, H. S.; Sethi, D. S. Absorption Cross Sections of CF_2 in the $\tilde{A}^1B_1$-$\tilde{X}^1A_1$ Transition at 0.5 nm Intervals and Absolute Rate Constant for 2 CF_2 → C_2F_4 at 298 ± 3 K. *J. Photochem.* **1987**, *38*, 1−13.

(27) Eden, S.; Limão-Viera, P.; Hoffmann, S. V.; Mason, N. J. VUV Photoabsorption by Hexafluoropropene. *Chem. Phys. Lett.* **2003**, *379*, 170−176.

(28) Astholz, D. C.; Brouwer, L.; Troe, J. High Temperature Ultraviolet Absorption Spectra of Polyatomic Molecules in Shock Waves. *Ber. Bunsenges. Phys. Chem.* **1981**, *85*, 559−564.

(29) Montgomery, J. A.; Frisch, M. J.; Ochterski, J. W.; Petersson, G. A. A Complete Basis Set Model Chemistry. VI. Use of Density Functional Geometries and Frequencies. *J. Chem. Phys.* **1999**, *110*, 2822−2827.
(30) Curtiss, L. A.; Redfern, P. C.; Raghavachari, K. Gaussian-4 Theory. *J. Chem. Phys.* **2007**, *126*, 084108−1−12.
(31) Curtiss, L. A.; Redfern, P. C.; Raghavachari, K. Gaussian-4 Theory Using Reduced Order Perturbation Theory. *J. Chem. Phys.* **2007**, *127*, 124105−1−8.
(32) Frisch, M. J.; Trucks, G. W.; Schlegel, H. B.; Scuseria, G. E.; Robb, M. A.; Cheeseman, J. R.; Scalmani, G.; Barone, V.; Menucci, B.; Petersson, G. A.; et al. *Gaussian 09, Revision A.02-SMP*; Gaussian Inc.: Wallingford, CT, 2009.
(33) Zazza, C.; Benciovenni, L.; Aschi, M. A Density Functional Theory Study of Hexafluoropropene: Low-Lying Singlet Excited States and Primary Photodissociation Channel. *Chem. Phys. Lett.* **2004**, *399*, 184−189.
(34) Just, Th.; Troe, J. Theory of Two-Channel Unimolecular Reactions. 1. General Formulation. *J. Phys. Chem.* **1980**, *84*, 3068−3072.
(35) Troe, J. Predictive Possibilities of Unimolecular Rate Theory. *J. Phys. Chem.* **1979**, *83*, 114−126.
(36) Cobos, C. J.; Troe, J. Theory of Thermal Unimolecular Reactions at High Pressures. II. Analysis of Experimental Results. *J. Chem. Phys.* **1985**, *83*, 1010−1015.
(37) Maergoiz, A. I.; Nikitin, E. E.; Troe, J.; Ushakov, V. G. Classical Trajectory and Statistical Adiabatic Channel Study of the Dynamics of Capture and Unimolecular Bond Fission. V. Valence Interactions between Two Linear Rotors. *J. Chem. Phys.* **1998**, *108*, 9987−9998.
(38) Troe, J.; Ushakov, V. G. Representation of "Broad" Falloff Curves for Dissociation and Recombination Reactions. *Z. Phys. Chem.* **2014**, *228*, 1−10.
(39) Troe, J. Theory of Thermal Unimolecular Reactions in the Falloff Range. I. Strong Collision Rate Constants. *Ber. Bunsenges. Phys. Chem.* **1983**, *87*, 161−169.
(40) Troe, J.; Ushakov, V. G. Revisiting Falloff Curves of Thermal Unimolecular Reactions. *J. Chem. Phys.* **2011**, *135*, 054304−1−10.
(41) Buravtsev, N. N.; Grigor'ev, A. S.; Kolbanovskii, Y. A. Kinetics of the Formation and Decomposition of Perfluorobutenes during Gas-Phase Pyrolysis of the Lower Perfluoroolefins. *Kinet. Catal.* **1989**, *30*, 386−390.
(42) Buravtsev, N. N.; Grigor'ev, A. S.; Kolbanovskii, Y. A. Kinetics and Mechanism of Pyrolysis of Hexafluoropropylene. *Kinet. Catal.* **1989**, *30*, 13−22.
(43) Ainagos, A. F. Mechanism and Kinetics of Pyrolysis of Perfluorohexane. *Kinet. Catal.* **1991**, *32*, 720−725.
(44) Lee, T. J.; Taylor, P. R. A Diagnostic for Determining the Quality of Single-Reference Electron Correlation Methods. *Int. J. Quantum Chem.* **1989**, No. Suppl. 23, 199−207.